

# Active control of sound transmission through a hole in a large thick wall

Xiaojun Qiu (1), Ming Qin (2) and Haishan Zou (3)

(1) Centre for Audio, Acoustics and Vibration, Faculty of Eng. and IT, University of Technology Sydney, Sydney, Australia

(2) Institute of Acoustics, Nanjing University, Nanjing 210093, China

(3) Institute of Acoustics, Nanjing University, Nanjing 210093, China

## ABSTRACT

Holes in walls of enclosures or buildings are often the weak link in the chain of sound insulation. This paper introduces an analytical model to calculate the sound transmission from a baffled rectangular hole based on the modal expansion approach, and proposes to install an active noise control system inside the hole to improve the transmission loss of the perforated wall. Different control source and error sensing strategies are investigated, and it is found that for a 30 cm thick wall with a 6 cm by 6 cm hole, an active control system with 1 control source and 1 error sensor can achieve more than 20 dB attenuation up to 2700 Hz, while that with a compound control source consisting of 4 loudspeakers, the system can achieve similar reduction up to 3900 Hz.

## 1 INTRODUCTION

Most noise control enclosures require some form of ventilation and they may also require access for passing materials in and out (Bies and Hansen 2009). Such necessary permanent openings or holes must be treated with some form of silencing to avoid compromising the effectiveness of the enclosures. In a good design, the acoustics performance of access silencing matches that of the wall of the enclosures. Usually, the silencers must be specially designed for these openings. The objective of this paper is to investigate the feasibility of applying active noise control in the holes so that no extra mufflers need to be used for the enclosures.

Sound transmission through apertures has been investigated intensively. For sound transmission through a large aperture (larger than wavelength) in a rigid plane screen of infinite extension, the Kirchhoff's integral was applied with an approximation that the sound field in the opening is essentially undisturbed by the diffraction wave from the aperture boundary so that the pressure and pressure gradient in the opening are set equal to those of the undisturbed primary sound field. For small apertures (smaller than wavelength), the volume velocity at the aperture opening can be obtained to calculate its sound radiation at the rear side of the wall (Kuttruff 2007, p.124). This paper focuses on small holes whose size is smaller than the sound wavelength.

Gompeters (1964) was the first to investigate the "sound insulation" of circular and slit-shaped apertures. Wilson and Soroka (1965) studied a circular aperture in a plane wall of finite thickness subjected to plane wave incidence with a numerical approach and compared the results with measurements carried out between two reverberant chambers. A normalized frequency,  $ka$  (where  $k$  is the wave number and  $a$  is the aperture radius), was used to make results independent of aperture dimensions. They also showed that above a given value (later on called "transition frequency"), depending on the ratio between the aperture thickness and its radius, almost all acoustic energy passed through the aperture. Conversely, below that frequency the energy transmitted decreased but, particularly when the opening was small compared to thickness, strong resonance phenomena appeared. Later on, Sauter and Soroka (1970) investigated the case of a rectangular opening under similar boundary conditions. Their study pointed out that these square apertures behaved nearly exactly as circular ones. However, depending on the aspect ratio of the opening, slight variations of the resonance phenomena were observed.

After such early-stage investigations, there are several papers studied this topic, which are introduced in the extensive review carried out by Sgard, Nelisse and Atalla (2007). They proposed a new numerical approach capable of handling diffuse field conditions and showed that the transmission coefficient at very low frequencies ( $ka < 0.3$ ) increased in presence of random incidence, while at high frequency ( $ka > 7$ ) the difference tended to fade. In between this interval the variation was strongly dependent on the aperture shape, but the increase never exceeded the low frequency correction. However, for larger and proportionate apertures the transition was very smooth. Such conclusions were further confirmed with the experimental measurements by Trompette and others (2009), and they showed that apertures having different aspect ratios but the same area had a similar transmission curve. Conversely, when the area was changed (and hence the equivalent radius) the expected transition frequency changed accordingly.

This paper introduces an analytical model to calculate the sound transmission from a baffled rectangular hole based on the modal expansion approach first, and then proposes to install an active noise control system inside the hole to improve the transmission loss of the perforated wall. Different control source and error sensing strategies are investigated.

## 2 MODEL

Figure 1 shows a configuration of the problem where there is a rectangular aperture with dimensions of  $2a \times 2b$  located in an infinite large rigid wall with a finite thickness of  $d$ . The primary point sound source is located outside the aperture while secondary point sound sources for active noise control are located inside the aperture.

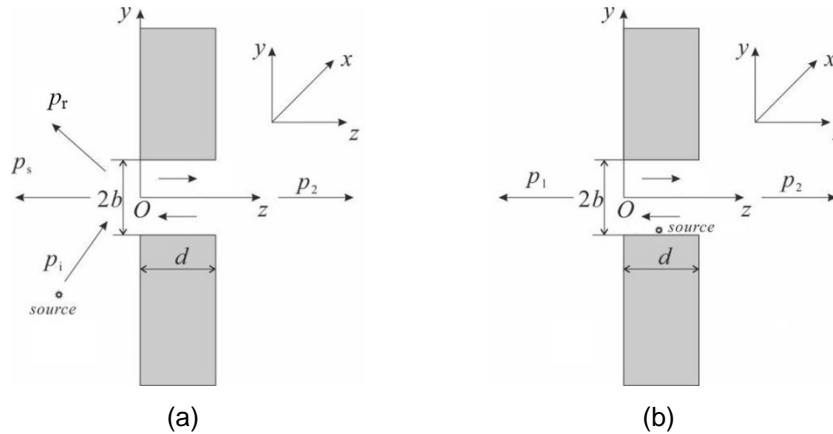


Figure 1: An aperture in an infinite large rigid wall with a finite thickness, (a) a primary point sound source outside the aperture, (b) a secondary point sound source inside the aperture.

The incident sound pressure at location  $\mathbf{r}$  generated by the primary source located at  $\mathbf{r}_p$  with source strength of  $q_p$  can be expressed by (Bies and Hansen 2009)

$$p_i(\mathbf{r}) = \frac{jk\rho c q_p}{4\pi|\mathbf{r}-\mathbf{r}_p|} e^{-jk|\mathbf{r}-\mathbf{r}_p|} \quad (1)$$

where  $k$  is wave number,  $\rho$  is the density of air and  $c$  is speed of sound. The overall sound pressure at the incident side of the aperture can be calculated by the superposition of the incidence wave, reflective wave and the scattering wave as (Sgard, Nelisse, and Atalla 2007)

$$p_1(\mathbf{r}) = p_i(\mathbf{r}) + p_r(\mathbf{r}) + p_s(\mathbf{r}) \quad (2)$$

The reflective and the scattering waves can be obtained by

$$p_r(\mathbf{r}) = \frac{jk\rho c q_p}{4\pi|\mathbf{r}-\mathbf{r}_r|} e^{-jk|\mathbf{r}-\mathbf{r}_r|} \quad (3)$$

$$p_s(\mathbf{r}) = \int_{S_1} G(\mathbf{r}, \mathbf{s}) \frac{1}{j\omega\rho_0} \frac{\partial p_1(\mathbf{s})}{\partial z} dS \quad (4)$$

where  $S_1$  is the aperture surface on the source side,  $\mathbf{r}_r$  is the location of the image source of the primary sound source regarding the infinite wall, and  $G(\mathbf{r}, \mathbf{s})$  is the Green function in the semi-infinite space at one side of the wall for a sound source located at  $\mathbf{s}$  on the aperture surface,

$$G(\mathbf{r}, \mathbf{s}) = \frac{j\omega\rho_0}{2\pi|\mathbf{r}-\mathbf{s}|} e^{-jk|\mathbf{r}-\mathbf{s}|} \quad (5)$$

Similarly, the sound radiated by the aperture into the free space behind the infinite wall is given by

$$p_2(\mathbf{r}) = -\int_{S_2} G(\mathbf{r}|\mathbf{s}) \frac{1}{j\omega\rho_0} \frac{\partial p_2(\mathbf{s})}{\partial z} dS \quad (6)$$

where  $S_2$  is the aperture surface on the radiation side. The sound field inside the aperture (a rigid cavity with two ends open) can be expressed by

$$p_a(\mathbf{r}) = \sum_{p,q} (A_{pq}^+ e^{-jk_{pq}z} + A_{pq}^- e^{jk_{pq}z}) \psi_{pq}(x, y) \quad (7)$$

where

$$\psi_{pq}(x, y) = \cos\left[\frac{p\pi(x+a)}{2a}\right] \cos\left[\frac{q\pi(y+b)}{2b}\right] \quad (8)$$

$$k_{pq} = \sqrt{k^2 - \left(\frac{p\pi}{2a}\right)^2 - \left(\frac{q\pi}{2b}\right)^2} \quad (9)$$

The normal particle velocity on both end surfaces of the aperture is proportional to its pressure gradient along  $z$  direction, which has the form of

$$\left. \frac{\partial p_a(\mathbf{r})}{\partial z} \right|_{z=0} = - \sum_{p,q} jk_{pq} (A_{pq}^+ - A_{pq}^-) \psi_{pq}(x, y) \quad (10)$$

$$\left. \frac{\partial p_a(\mathbf{r})}{\partial z} \right|_{z=d} = - \sum_{p,q} jk_{pq} (A_{pq}^+ e^{-jk_{pq}d} - A_{pq}^- e^{jk_{pq}zd}) \psi_{pq}(x, y) \quad (11)$$

By using the normal particle velocity continuity condition on both sides of the aperture at the end surfaces, the sound radiated by the aperture to both sides of the wall can be written as

$$p_s(\mathbf{r}) = - \sum_{p,q} \frac{k_{pq}}{k\rho_0 c_0} (A_{pq}^+ - A_{pq}^-) \int_0^a \int_0^b G(\mathbf{r} | (u, v)) \psi_{pq}(u, v) du dv \quad (12)$$

$$p_2(\mathbf{r}) = \sum_{p,q} \frac{k_{pq}}{k\rho_0 c_0} (A_{pq}^+ e^{-jk_{pq}d} - A_{pq}^- e^{jk_{pq}zd}) \int_0^a \int_0^b G(\mathbf{r} | (u, v)) \psi_{pq}(u, v) du dv \quad (13)$$

By using the pressure continuity condition on both sides of the aperture at the end surfaces, it has

$$p_i(x, y, 0) + p_r(x, y, 0) + p_s(x, y, 0) = \sum_{p,q} (A_{pq}^+ + A_{pq}^-) \psi_{pq}(x, y) \quad (14)$$

$$p_2(x, y, d) = \sum_{p,q} (A_{pq}^+ e^{-jk_{pq}d} + A_{pq}^- e^{jk_{pq}zd}) \psi_{pq}(x, y) \quad (15)$$

Substituting the primary incidence pressure  $p_i(\mathbf{r})$ , the reflective wave  $p_r(\mathbf{r})$ , Eqs. (12) and (13) into Eqs. (14) and (15), multiplying all the equations by  $\psi_{mn}(x, y)$ , and then integrating over the respective surfaces of the aperture lead to,

$$F_{mn} - \sum_{p,q} jk_{pq} (A_{pq}^+ - A_{pq}^-) Z_{pqmn} = (A_{mn}^+ + A_{mn}^-) \Lambda_{mn} \quad (16)$$

$$\sum_{p,q} jk_{pq} (A_{pq}^+ e^{-jk_{pq}d} - A_{pq}^- e^{jk_{pq}zd}) Z_{pqmn} = (A_{mn}^+ e^{-jk_{mn}d} + A_{mn}^- e^{jk_{mn}d}) \Lambda_{mn} \quad (17)$$

where  $\Lambda_{mn} = \varepsilon_m \varepsilon_n ab$ ,  $\varepsilon_0 = 2$  and  $\varepsilon_m = 1$  for  $m \neq 0$ , and

$$F_{mn} = \int_{-a}^a \int_{-b}^b \frac{jk\rho c q_p}{2\pi |\mathbf{s} - \mathbf{r}_p|} e^{-jk|\mathbf{s} - \mathbf{r}_p|} \psi_{mn}(x, y) dx dy \quad (18)$$

$$Z_{pqmn} = \int_{-a}^a \int_{-b}^b \int_{-a}^a \int_{-b}^b \frac{e^{-jk\sqrt{(x-u)^2 + (y-v)^2}}}{2\pi\sqrt{(x-u)^2 + (y-v)^2}} \psi_{pq}(u, v) \psi_{mn}(x, y) du dv dx dy \quad (19)$$

is a specific radiation impedance, which can be calculated numerically or with an approximate expression (Sha, Yang and Gan 2005). The modal magnitudes for all aperture modes can be obtained by solving Eqs. (16) and (17), which can be further substituted to Eq. (13) to obtain the transmitted sound. The transmitted power from the opening can be calculated by carrying out an intergration of the real part of the sound intensity on the radiation side surface of the aperture as

$$W_a(\mathbf{r}_p) = \frac{1}{2} \text{Re} \left\{ \int_{S_2} p_2(\mathbf{s}) v_2^*(\mathbf{s}) dS \right\} \quad (20)$$

where the normal particle velocity along the z direction can be obtained from Eq. (11).

For a control source located at  $\mathbf{r}_c = (x_c, y_c, z_c)$  in the aperture shown in Figure 1(b), the sound pressure in the aperture has an extra source term in addition to that in Eq. (7), and can be expressed as

$$p_c(\mathbf{r}) = \sum_{p,q} (A_{pq}^+ e^{-jk_{pq}z} + A_{pq}^- e^{jk_{pq}z} + \frac{\rho\omega q_c e^{-jk_{pq}z-z_c} \psi_{pq}(x_c, y_c)}{2k_{pq} \Lambda_{pq}}) \psi_{pq}(x, y) \quad (21)$$

Similarly, the modal magnitudes for all aperture modes generated by the control source can be calculated as well as the transmitted sound and power to the radiation side of the wall. Because this is no incidence sound from the source side, so  $p_1(\mathbf{r})$  in Eq. (2) only contains the scattering term  $p_s(\mathbf{r})$  in the calculation.

The total sound pressure with active control is superstitution of both the primary sound and the control sound,

$$p_t(\mathbf{r}) = p_p(\mathbf{r}) + Z_{ce}(\mathbf{r})q_c \quad (22)$$

where  $p_p(\mathbf{r})$  is the primary sound pressure at location  $\mathbf{r}$ , and  $Z_{ce}(\mathbf{r})$  is the transfer function from the source strength of the control source to the sound pressure at location  $\mathbf{r}$ . All these can be calculated by the above established model. The objective of the control is to reduce the total radiation power from the aperture to the radiation side, and different cost functions can be used for obtaining the optimal strength of the secondary source. For example, the summation of the squared total sound pressure at  $N_e$  error locations can be used as the cost function,

$$J_p = \sum_{i=1}^{N_e} |p_t(\mathbf{r}_i)|^2 + \beta q_c^2 \quad (23)$$

where  $\beta$  is a positive real number to constrain the strengths of control source. For multiple control sources to reduce the sound pressure at multiple error locations, Eqs. (22) and (23) can be written in matrix form as

$$\mathbf{p}_t = \mathbf{p}_p + \mathbf{Z}_{ce} \mathbf{q}_c \quad (24)$$

$$J_p = \mathbf{p}_t^H \mathbf{p}_t + \beta \mathbf{q}_c^H \mathbf{q}_c = \mathbf{q}_c^H (\mathbf{Z}_{ce}^H \mathbf{Z}_{ce} + \beta \mathbf{I}) \mathbf{q}_c + \mathbf{q}_c^H \mathbf{Z}_{ce}^H \mathbf{p}_p + (\mathbf{Z}_{ce}^H \mathbf{p}_p)^H \mathbf{q}_c + \mathbf{p}_p^H \mathbf{p}_p \quad (25)$$

where the superscript H denotes the Hermittan transpose,  $\mathbf{p}_p$  is the vector of the primary sound pressure at  $N_e$  error locations,  $\mathbf{q}_c$  is the vector of the source strength of  $N_c$  control sources, while  $\mathbf{Z}_{ce}$  is the transfer function matrix, whose elements are transfer functions from all control sources to all error sensors. The optimal control source strength that minimizes the above cost function can be calculated by (Hansen et al 2013)

$$\mathbf{q}_c^o = -(\mathbf{Z}_{ce}^H \mathbf{Z}_{ce} + \beta \mathbf{I})^{-1} \mathbf{Z}_{ce}^H \mathbf{p}_p \quad (26)$$

With the optimal control source strength, the sound field with active control as well as the total radiation power from the aperture to the radiation side can be calculated. Of course, it is also possible to directly use the radiation power from the aperture to the radiation side as the cost function to calculate the optimal control source strength, which provides an upper limit performance for the specified control source configuration despite of error sensing strategies and configurations. Different control source and error sensor configurations are investigated via simulations in the next section.

### 3 SIMULATIONS

The 30 cm long rectangular aperture used in the simulations has cross section dimensions of 6 cm by 6 cm. The cutoff frequency for the plane wave propagation in the aperture duct is about 2858 Hz; however the simulations are carried out up to 5000 Hz to cover most frequency range of practical noise. In the simulations, one or several point sources located at different positions on the source side are used to mimic the primary noise source, while one, two or four point sources located on the internal boundaries at the centre of the duct act as the control source (Qin, 2017). For the two control loudspeaker case, the two loudspeakers are located on the opposite sides instead of the neighbouring sides inside the duct to generate symmetrical sound field for controlling plane waves; while for the four control loudspeaker case, each loudspeaker is located on a different internal surface of the duct. The reliability of the proposed analytical model was validated first by using commercial software, and then the model was used in the active noise control simulations because it runs much faster than the commercial software.

#### 3.1 Validation of the Analytical Model

The analytical model described in Section 2 was validated first by using commercial software LMS Virtual Lab12. Figure 2(a) shows the Finite Element Model built in the software, where the duct in the middle has the dimensions mentioned above, and two hemispheres with a diameter of 0.22 m were configured as Automatically Matched Layers and used outside the two openings to simulate baffled radiation to semi-infinite space. Figure 2(b) compares the sound pressure levels at (-0.1, 0.08, 0.42) m calculated with the proposed analytical model and the commercial software for a primary point source located at (-0.04, -0.03, -0.1) m. It is clear the results calculated from the analytical model agree reasonably well with that from the commercial software. In the calculation with the analytical model, the order of the modes is selected to 8.

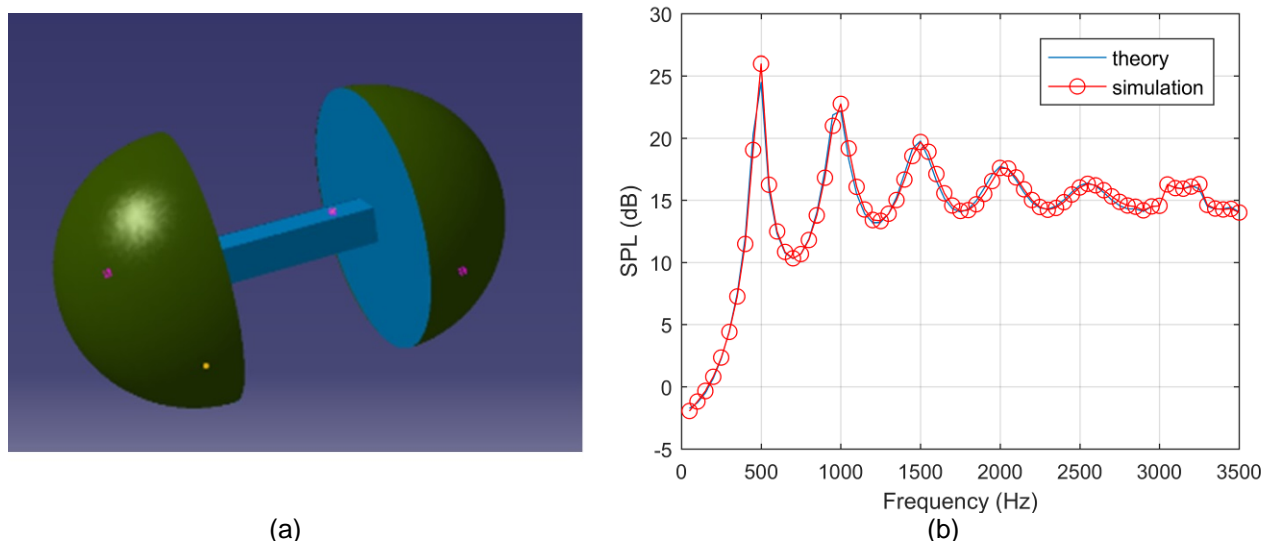


Figure 2: (a) The Finite Element Model built with LMS Virtual. Lab12, (b) the sound pressure levels at (-0.1, 0.08, 0.42) m calculated with the proposed analytical model and the commercial software for a primary point source located at (-0.04, -0.03, -0.1) m.

#### 3.2 Effects of Control Source Configurations

The first set of simulations are used to investigate the effects of control source configurations on the performance of the ANC system, so the radiated sound power from the aperture to the radiation side is used as the cost function to calculate the optimal control source strength. This provides an upper limit performance for the specified control source configuration despite of error sensing strategies and configurations. It should be noted here that only single channel active control system is used in the simulations for its low cost. Although 2 or 4 loudspeakers are used in this case, they are all driven by a single controller output as a single compound control source. The benefit of using a compound control source is its capability of generating symmetrical sound field inside the duct.

Figure 3(a) shows the radiated sound power from the aperture to the radiation side with and without active control for a primary sound source located at (0, 0, -1.0) m with a source strength of  $10^{-4}$  kg/s<sup>2</sup>, where the control loudspeakers are located at the centre of the duct on different internal sides. Figure 3(b) gives the corresponding noise reduction with 1, 2 and 4 control loudspeakers where the noise reduction is defined as the difference between the radiated sound power from the aperture to the radiation side with and without active control. It is clear that using only one control loudspeaker can reduce the sound power transmitted from the hole up to the cutoff frequency for the plane wave propagation in the aperture duct, which is about 2858 Hz. The noise reduction at

most frequencies below this frequency can be up to 50 dB. When two or four control loudspeakers (as a single compound source) are used, the effective control frequency can be shifted to higher frequency because symmetrical control sound fields can be generated with more loudspeakers above the cutoff frequency.

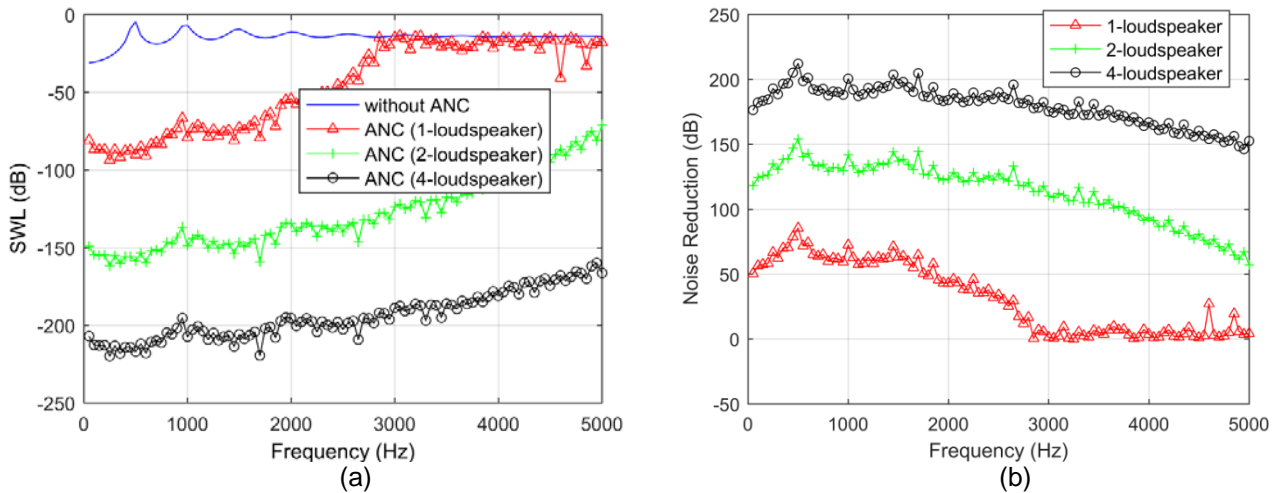


Figure 3: For a primary sound source located at  $(0, 0, -1.0)$  m with a source strength of  $10^{-4}$  kg/s<sup>2</sup>, (a) the radiated sound power from the aperture to the radiation side with and without active control, (b) the noise reduction with 1, 2 and 4 loudspeakers (as a compound source) located at the centre of the duct on different internal sides.

It should be noted that it is usually impossible to have noise reduction of more than 30 dB in practice, so the simulation results of more than 30 dB are just an indication of large reduction and can be treated as some value like 30 dB in practice. The primary sound field for the simulations in Figure 3 is generated by a primary point sound source located on the axis of the duct opening, so it is symmetrical. This is the reason that the compound control source consisting of 2 or 4 loudspeakers provides better control above the cutoff frequency up to 5000 Hz. In practical applications, the noise might come from many directions, and the benefits would not be such large, as shown in Figure 4, where then noise reduction for a primary sound source located at 1.0 m away from the duct opening but from different direction of  $(0^\circ, 0^\circ)$  or  $(30^\circ, 30^\circ)$  are given. Similar to that with only one loudspeaker, a compound source consisting of 4 control sources cannot have significant noise reduction above the cutoff frequency either for the primary sound from  $(30^\circ, 30^\circ)$  direction.

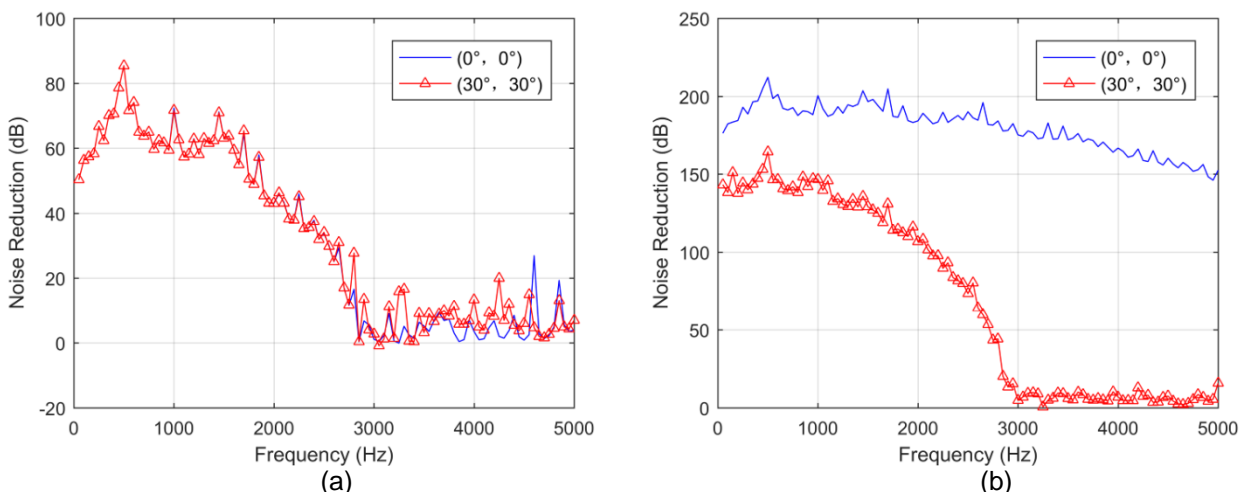


Figure 4: Noise reduction for a primary sound source located at 1.0 m away from the duct opening but in the direction of  $(0^\circ, 0^\circ)$  or  $(30^\circ, 30^\circ)$ , (a) using 1 control loudspeaker located at the centre of the duct, (b) using a compound control source consisting of 4 loudspeakers located at the centre of the duct on different internal sides.

Figure 5 shows noise reduction for different primary sound fields consisting of 1 or 13 point sources at 0.1 m (near field) or 4.0 m (far field) away from the duct opening using 1 control loudspeaker or a compound control source consisting of 4 loudspeakers located at the centre of the duct on different internal sides. For the 1 point source that is used to generate the primary sound field, the point source is located on the axis of the duct opening; while the 13 point sources that are used for generating the primary sound field are distributed non-evenly on the hemisphere to

mimic random incidence sound field. For the ANC system with one loudspeaker, the performance remains similar for different primary sound fields and is only effective below the cutoff frequency of the duct; while for the compound source consisting of 4 loudspeakers, the performance is better than that with one loudspeaker but also deteriorates significantly above the cutoff frequency.

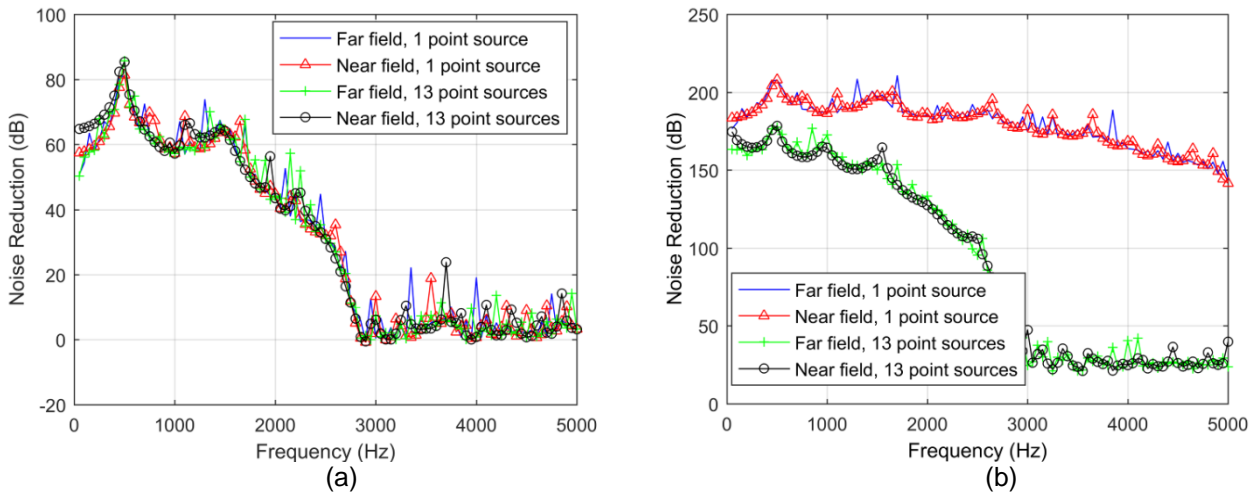


Figure 5: Noise reduction for different primary sound fields consisting of 1 or 13 point sources at 0.1 m (near field) or 4.0 m (far field) away from the duct opening, (a) using 1 control loudspeaker located at the centre of the duct, (b) using a compound control source consisting of 4 loudspeakers located at the centre of the duct on different internal sides.

### 3.3 Effects of Error Sensor Configurations

Although the control objective is to reduce the radiated sound power from the aperture to the radiation side, it is difficult to use this cost function practically. This subsection investigates the efforts of error sensor configurations, which install several microphones at the opening of the duct to the radiation side. The sound pressure signals picked up by these microphones are fed to the controller so that the control algorithm can minimise the sum of the squared sound pressures at these positions. Although the controller is tuned by minimising the cost function, the noise reduction performance of the ANC system is still evaluated by the radiated sound power from the aperture to the radiation side.

In the simulations, the primary sound field is generated by 13 point sources at 4 m away from the duct opening of the source side. The error microphones are located on a cross section inside the duct about 6 cm away from the radiation side opening. Figure 6 shows the noise reduction by using 1 error microphone which is located at the centre of the cross section and 9 error microphones which are evenly distributed on the cross section. It shows that 1 or 9 error microphones can give similar noise reduction for the 1 control loudspeaker case, while 9 error microphones can give better performance for the compound control source consisting of 4 control loudspeakers.

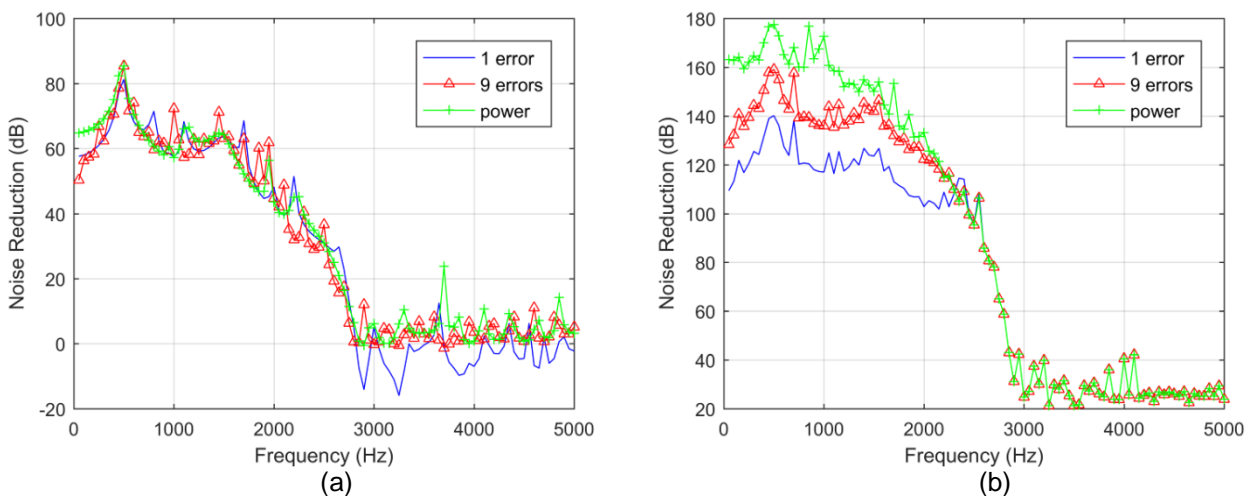


Figure 6: Noise reduction with different cost error sensor configurations (a) using 1 control loudspeaker located at the centre of the duct, (b) using a compound control source consisting of 4 loudspeakers located at the centre of the duct on different internal sides.

Figure 7 shows the noise reduction with 1 error microphone at different positions and that with 4 error microphones on the middle of the four side boundary lines on the cross section. For the one control loudspeaker case, it is clear that putting one error microphone in the corner or using 4 error microphones provides reasonable noise reduction below the cutoff frequency without introducing significant noise amplification (minus noise reduction) in the high frequency range. For the compound control source consisting of 4 loudspeakers, the noise reduction performances with different error sensor configurations are similar.

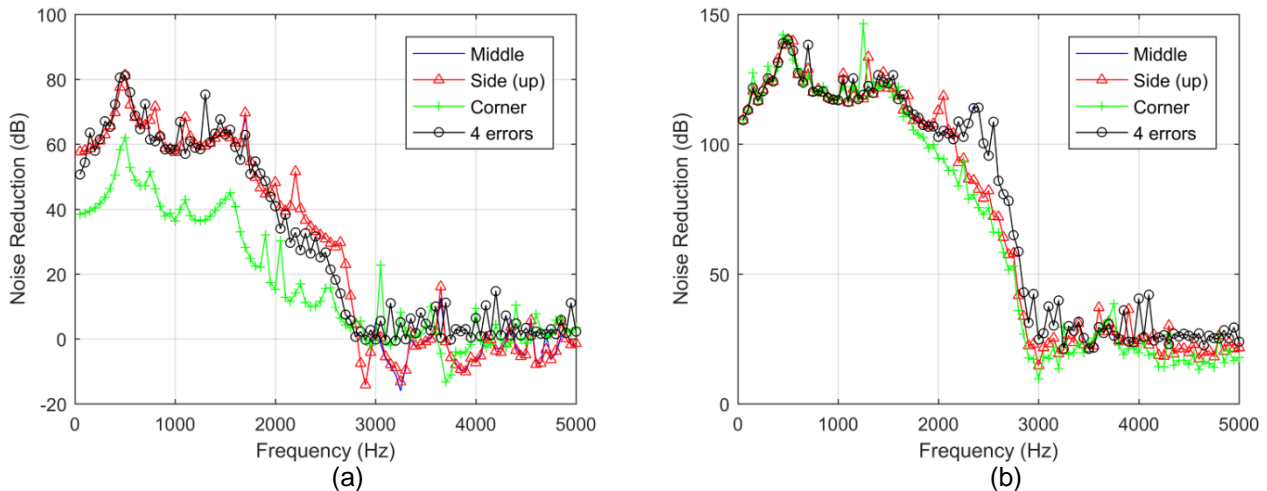


Figure 7: Noise reduction with different cost error sensor locations (a) using 1 control loudspeaker located at the centre of the duct, (b) using a compound control source consisting of 4 loudspeakers located at the centre of the duct on different internal sides.

#### 4 CONCLUSIONS

This research investigates active control of sound transmission through a hole in a large thick wall. An analytical model for calculating the sound transmission from a baffled rectangular hole is introduced first based on the modal expansion approach, and then an active noise control system is proposed to be installed inside the hole to improve the transmission loss of the wall. Different control source and error sensing strategies are investigated, and it is found that for a 30 cm thick wall with a 6 cm by 6 cm hole, an active control system with 1 control source and 1 error sensor can achieve more than 20 dB attenuation up to 2700 Hz. It is concluded that a single channel ANC system with 1 control source and 1 error sensor can provide effective control up to the cutoff frequency of the hole.

#### ACKNOWLEDGEMENTS

This work was supported under Australian Research Council's Linkage Projects funding scheme (LP140100987) and National Nature Science Foundation of China (Projects 11474163).

#### REFERENCES

- Bies, David A. and Colin H. Hansen. 2009. *Engineering Noise Control: Theory and Practice*. 4th ed. CRC Press.
- Gompeters, M.C. 1964. "The 'sound insulation' of circular and slit-shaped apertures." *Acta Acustica united with Acustica* 14(1): 1-16.
- Hansen, C. H., S. D. Snyder, X. Qiu, et al. 2013. *Active Control of Noise and Vibration*, 2nd ed. CRC Press.
- Kuttruff, H. 2007. *Acoustics: An Introduction*, Taylor & Francis.
- Wilson, G. P. and W. W. Soroka. 1965. "Approximation to the diffraction of sound by a circular aperture in a rigid wall of finite thickness." *Journal of the Acoustical Society of America* 37(2): 287-297.
- Sauter, A. and W. W. Soroka. 1970. "Sound transmission through rectangular slots of finite depth between reverberant rooms." *Journal of the Acoustical Society of America* 47(1): 5-11.
- Sgard, F., H. Nelisse, and N. Atalla. 2007. "On the modeling of the diffuse field sound transmission loss of finite thickness apertures." *Journal of the Acoustical Society of America* 122(1): 302-313.
- Trompette, N., J -L Barbry, F. Sgard, and H. Nelisse. 2009. "Sound transmission loss of rectangular and slit-shaped apertures: Experimental results and correlation with a modal model." *Journal of the Acoustical Society of America* 125(1): 31-41.
- Sha, K., J. Yang and W. S. Gan. 2005. "A simple calculation method for the self-and mutual-radiation impedance of flexible rectangular patches in a rigid infinite baffle." *Journal of Sound and Vibration* 282: 179-195.
- Qin, M. 2017. "Active Control of The Sound Transmission through a Baffled Opening." master degree theses, Nanjing University.